Combustion and Flame 219 (2020) 339–348

Contents lists available at ScienceDirect

Combustion and Flame

journal homepage: www.elsevier.com/locate/combustflame

Analysis of mixture stratification effects on unstrained laminar flames

E. Inanc[a,*], N. Chakraborty[b], A.M. Kempf[a]

[a] Chair of Fluid Dynamics, Institute for Combustion and Gasdynamics (IVG), University of Duisburg-Essen, Germany
[b] School of Engineering, Newcastle University, Claremont Road, Newcastle-Upon-Tyne NE1 7RU, UK

ARTICLE INFO

Article history:
Received 3 February 2020
Revised 3 June 2020
Accepted 3 June 2020

Keywords:
Equivalence ratio stratification
Unstrained laminar flames
Oscillation
Flame speed
Flame thickness

ABSTRACT

Detailed one-dimensional computations of unsteady unstrained laminar flames subjected to sinusoidal equivalence ratio perturbations are presented. The responses of the flame thickness, flame speeds, species concentrations and the species reaction rates to equivalence ratio variations are investigated. The effect of stratification is quantified by comparing the structure of a stratified flame to that of an equivalent homogeneous mixture flame at an equivalence ratio that the stratified flame experiences. The difference between a flame burning into a leaner mixture or a richer mixture yields hysteresis for consumption speed and flame thickness in the equivalence ratio space, which becomes more prominent with stronger stratification, especially when the flame propagates towards a negative equivalence ratio gradient under fuel-lean conditions. The displacement speed and its components are analysed, with the diffusion, reaction rate and cross-dissipation components all showing a strong hysteresis, but with different signs, partially cancelling each other. The phase space responses of the scalars are compared and the different phase shifts are evaluated. Interestingly, these observations were not affected by the choice of the reaction mechanism. The effects of equal and mixture-average diffusivity assumptions on the results are tested, where the latter caused two times stronger hysteresis effects: the thermo-diffusive effects of heat and products behind the flame were found to play a significant role for laminar flame propagation in stratified mixtures, even for unstrained flames. The stratified flame shows significant alteration in the species concentrations and reaction rates, especially for the minor and product species. The response of the sinusoidal oscillations is compared against cases with linear mixture stratification. Even with the absence of the compressible strain, it is demonstrated that the stratification effects heavily influence the flame properties and the treatment of thermo-physical transport properties has been demonstrated to be pivotal to the accurate prediction of this behaviour.

1. Introduction

Stratified combustion can help to meet the strict emission requirements for internal combustion engines and gas turbines. Stratification can occur implicitly due to insufficient premixing of the fuel and the oxidiser or explicitly through multiple injections or staged combustion. Compared to homogeneous premixed combustion, the equivalence ratio stratification affects the local flame properties and may enhance flame propagation and lower emissions [1]. To study stratified combustion, experiments [2,3] and numerical methods [4–9] have been applied. A detailed overview is provided in the review paper by Lipatnikov [1].

The flame may either propagate normal to the equivalence ratio gradient, which is typically observed in triple-flame structures [10], or burn in gradient direction, which has been investigated for its influences on flammability limits [11], flame propagation speeds [5] and flame structure for various fuels including hydrogen [9], methane [12] and iso-octane [13]. The flame propagation in the direction of the equivalence ratio gradient can be examined in one dimension by analysing oscillation responses. The unsteady response of strained flames to velocity [4] and mixture composition [6] oscillations have been documented before, but the response of the flame propagation under unstrained conditions in one dimension is yet to be analysed in detail and the present paper addresses this void in the existing literature.

Industrially relevant stratified flames are usually fuel-lean, and the flame may burn into an even leaner mixture, which is referred to as back-supported (BS) combustion, or into a richer mixture closer to stoichiometry, which may be called front supported (FS). A fuel-lean BS flame propagates faster and has a thinner reaction zone [7] than a homogeneous mixture flame at the same (local) equivalence ratio. This is due to the relatively high heat and (radi-

* Corresponding author.
E-mail address: eray.inanc@uni-due.de (E. Inanc).

https://doi.org/10.1016/j.combustflame.2020.06.009
0010-2180/

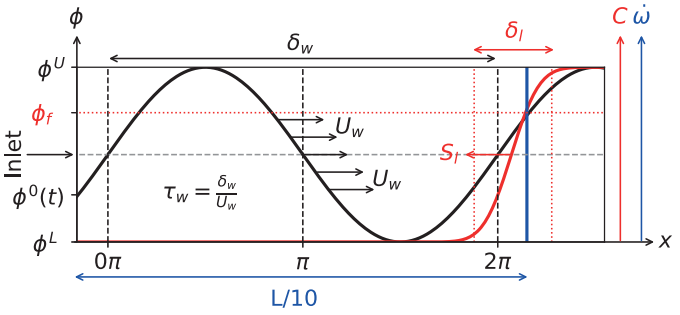

Fig. 1. Schematic of the stratified flame propagating in a sinusoidal equivalence ratio field with important parameters. (Not drawn to scale.) (For interpretation of the references to color in this figure legend, the reader is referred to the web version of this article.)

cal) species concentrations on the burnt side of the flame diffusing into the leaner preheat zone. As a result, the flammability limits of a flame in a stratified mixture can be extended [5].

Studying stratified mixture combustion in one-dimension is not trivial, as many solvers do not support unsteady solutions, and the resulting computational cost is surprisingly high. A common method to analyse stratification effects is to artificially constrain the flame to the stratification layer by introducing compressible strain in a counter-flow configuration [8], which limits such studies to (strongly) strained cases. This is problematic for studies where the equivalence ratio gradients occur more naturally, without imposed straining (e.g. in the Darmstadt and Cambridge Flames [2,3]). Another method allows for the flame to propagate through an equivalence ratio gradient [5], but, diffusion diminishes the equivalence ratio gradients, yielding a rapid reduction of the stratification effect.

The present work takes a different approach which, albeit computationally expensive, avoids these problems: a sinusoidal equivalence ratio field is generated by suitable unsteady inflow conditions, and a premixed stratified flame is initialised to freely propagate through the mixture. This work aims to (i) analyse the unsteady response of an unstrained flame to mixture stratification oscillations, to (ii) test the influences of the diffusivity assumptions and the reaction mechanisms on the results, and to (iii) propose and demonstrate the usefulness of an alternative consumption speed definition that is applicable for stratified flames.

2. Computational setup

To prepare the work presented here, the numerical experiment by Cruz et al. [5] was reproduced first to ensure the quality of our numerical techniques. A very good agreement was obtained, which is not shown here for the sake of brevity, however, can be found in the supplementary material.

One-dimensional unsteady unstrained laminar flames propagating through a sinusoidal methane-air mixture at 300 K in atmospheric conditions are calculated, as sketched in Fig. 1. The upper and lower limits of equivalence ratio are ϕ^U and ϕ^L, which are chosen as stoichiometric and fuel-lean, respectively.

The inlet velocity is controlled to establish a stabilised flame 4 mm from the inlet (approximately nine laminar flame thicknesses) in a homogeneous mixture at the equivalence ratio $\overline{\phi} = 0.85$, so that the preheat zone is not affected by the boundary conditions. The stratification oscillation around $\overline{\phi}$ is then introduced by modulating the inlet fuel mass flow-rate that matched the desired inlet equivalence ratio $\phi^0(t)$ with a sine function of period τ_w, velocity U_w, wavelength $\delta_w = U_w \cdot \tau_w$, frequency $f = 1/\tau_w$ and amplitude $A = (\phi^U - \phi^L)/2$:

$$\phi^0(t) = \overline{\phi} + A \cdot sin(2\pi f t) \quad (1)$$

The amplitude A yields the oscillations to remain in the fuel-lean side. It should be noted that the mass fraction of the oxidiser changes as the mass fraction of the fuel is modified to bring about the change in the equivalence ratio. A fixed inlet velocity is chosen in such a manner that the flame would oscillate around its initial location. To simplify the discussion of the results, velocity, period and wavelength are normalised with respect to the laminar flame speed S_l, flame time τ_l and flame thickness δ_l. As these values fluctuate in a stratified flame, fixed approximate values from a homogeneous premixed flame at $\phi = 0.85$ are used for normalisation. Hence, $S_l = 0.25$ m/s and $\delta_l = 0.5$ mm, respectively yielding a chemical timescale of $\tau_l = \delta_l / S_l$ of 2 ms.

Two cases with a linear mixture stratification layer are also tested, and are used as references. The flame that exhibits a linear negative equivalence ratio gradient is denoted as LBS and a positive one as LFS. The former case starts burning from a mixture of ϕ^U to ϕ^L, where the latter case is the opposite.

The simulations were performed with the in-house solver PsiPhi [14–17], originally developed for large-eddy simulations. The governing equations for mass, momentum, sensible enthalpy and species transport were solved (without sub-grid modelling) with a low-storage explicit Runge–Kutta scheme in low-Mach number formulation. Different cell sizes, domain lengths and time step sizes were tested to find an optimum setup for each case. The grid resolution dependency on the results was identified for OH mass fractions from one-dimensional laminar stoichiometric methane-air mixture simulations using 50, 25 and 12.5 µm cell sizes. The simulations with 50 and 25 µm achieved 1.6% and 1% relative differences to the results with 12.5 µm grid cell, respectively. The domain length $L = 40$ mm was resolved by 1600 equally sized cells of 25 µm.

Each simulation required 2000 or 20,000 CPUh on 24 cores depending on the chosen diffusivity assumption. The time step size was as low as 4 ns, limited by the diffusion time-step criterion. The equal diffusivity assumption was a factor of ten computationally cheaper due to the larger time step size (40 ns). Each case was simulated over three wavelengths (6π) to check for convergence and repeatability. The first wave period involved the unsteady transition of a homogeneous premixed flame to a stratified one.

An Augmented Reduced Mechanism (ARM) for methane/air combustion of 19 transported and 11 quasi-steady-state species by Lu and Law [18] (LL19) is employed. To check for the sensitivity of stratification phenomena to the reaction mechanism, the GRI3.0 [19] mechanism for the equal diffusivity cases was also tested. No significant difference was found, and only the results from LL19 are presented here. A brief discussion is given in Appendix B.

Two diffusivity assumptions are tested: (i) the equal diffusivity assumption sets the mass diffusivity of all chemical species to the thermal diffusivity, i.e. unity Lewis number, which is estimated from the local mixture properties. (ii) The mixture-average diffusivity assumption employs individual mass diffusivity for each species that depends on the temperature and the thermal differential diffusion. The former assumption is typically used for modelling turbulent stratified combustion cases, e.g. [20].

3. Definitions and equations

A stratification indicator $\lambda = \delta_w / \delta_l$ is considered as the equivalence ratio wavelength over the laminar flame thickness. A value of $\lambda \approx 3$ is typical of the stratification layer of the well-known Cambridge turbulent stratified flame experiment [3]. Similarly, a stratification thickness δ_S is introduced as $\delta_S = (\phi^U - \phi^L)/|\nabla\phi|_{max}$. The stratification indicator λ is estimated a priori, whereas the stratification thickness δ_S provides a posteriori quantification of the stratification strength.

Table 1
Overview of tested cases. The first letter of each name denotes if the case consists of a sinusoidal wave for *S* or a linear wave for *L*.

Name	diff.	mech.	ϕ_f^L	ϕ_f^U	U_w/S_l	τ_w/τ_l	λ	f/Hz	δ_s/δ_l
S1LL	equal	LL19	0.849	0.851	1.0	1.25	1.25	400	0.23
S2LL	equal	LL19	0.849	0.851	1.0	1.67	1.67	300	0.30
S3LL	equal	LL19	0.847	0.853	1.0	2.5	2.5	200	0.48
S4LL	equal	LL19	0.842	0.858	1.0	3.33	3.33	150	0.60
S5LL	equal	LL19	0.82	0.88	1.0	5	5	100	0.92
S10LL	equal	LL19	0.76	0.94	1.0	10	10	50	2.32
S40LL	equal	LL19	0.7	1.0	1.0	40	40	12.5	4.75
S5LD	mixt.	LL19	0.8	0.87	1.2	4.2	5	100	0.97
S10LD	mixt.	LL19	0.73	0.92	1.2	8.3	10	50	2.42
S40LD	mixt.	LL19	0.68	0.97	1.2	33.3	40	12.5	4.71
S5LG	equal	GRI3	0.82	0.88	1.0	5	5	100	0.92
S10LG	equal	GRI3	0.76	0.94	1.0	10	10	50	2.32
S40LG	equal	GRI3	0.7	1.0	1.0	40	40	2.5	4.68
LBS	equal	LL19	0.7	1.0	1.0	0.6	0.6	–	0.52
LFS	equal	LL19	0.7	1.0	0.8	0.75	0.6	–	0.48

The local equivalence ratio ϕ is computed from the local mixture fraction ζ defined by Bilger [21]. For further details, please refer to Appendix A and Eqs. (A.1) and (A.2). This equivalence ratio allows an unambiguous definition of the composition in the flame [5]. The equivalence ratio ϕ_f that the flame experiences corresponds to the location of the highest heat release within the flame. For short wavelengths δ_w, the diffusive fluxes can reduce the amplitude of stratification, so that the flame experiences different upper and lower limits in comparison to those set at the inlet; they are labelled as ϕ_f^U and ϕ_f^L, respectively. The aforementioned information is summarised in Table 1.

For a premixed flame, reaction progress variable can be defined as $C = (Y_R^u - Y_R)/(Y_R^u - Y_R^b)$: The indices u and b denote the mass fraction values in the fresh reactants and fully burned products, respectively, and R denotes the reactants. Therefore, the reaction rate of the reaction progress variable can be expressed as $\dot{\omega}_C = -\dot{\omega}_R/(Y_R^u - Y_R^b)$, where $\dot{\omega}_R$ is the reaction rate of the reactants. In stratified flames, the values in the fresh reactants and fully burned products are not fixed, hence, the local equivalence ratio can be used to define these quantities. Thus for stratified flames, C can be defined in the following manner in terms of oxygen (as reactant) mass fraction as:

$$C = \frac{Y_{O2}(\phi)_P^u - Y_{O2}}{Y_{O2}(\phi)_P^u - Y_{O2}(\phi)_P^b} \tag{2}$$

The unburnt Y^u and burnt Y^b mass fractions are taken from steady unstretched laminar homogeneous mixture flame calculations at the local equivalence ratio of the unsteady flames, indicated by subscript P (perfectly premixed). Three ranges of the progress variable will be considered in the discussion: the preheat zone $0.02 < C < 0.6$, the inner reaction zone $0.6 < C < 0.85$, and the burnout zone $0.85 < C < 0.98$. The ranges of C considered here for demarcating different flame zones are guided by previous a priori analyses [20]. The change in the definition of reaction progress variable may alter the ranges of C used for demarcating different zones within the flame. However, this is done as a post-processing exercise because a transport equation for C is not solved but C is constructed from the mass fraction fields and thus choices of C ranges for the different zones do not alter the results presented here. Indeed, the analysis has been performed using fuel mass fraction Y_{CH4} for the definition of C, but the results are omitted for brevity since the qualitative outcome is the same.

The conventional definition of the consumption speed of a species α in the case of fuel-lean or stoichiometric mixture (i.e. for $\phi \leq 1.0$) is given in terms of the reaction rate of this species $\dot{\omega}_\alpha$, unburnt density ρ^u and species mass fraction in the unburnt mixtures Y_α^u (because $Y_\alpha^b = 0$ for fuel-lean/stoichiometric combustion) as [5]:

$$S_{c,\alpha} = \frac{1}{\rho^u \cdot Y_\alpha^u} \int_{-\infty}^{+\infty} -\dot{\omega}_\alpha dx \tag{3}$$

For fuel-lean/stoichiometric premixed flames, this Eq. (3) can be rewritten as:

$$S_{c,\alpha} = \int_{-\infty}^{+\infty} \frac{\dot{\omega}_C}{\rho^u} dx \tag{4}$$

where $\dot{\omega}_C = -\dot{\omega}_\alpha / Y_\alpha^u$ is the reaction rate of reactant based reaction progress variable C for fuel-lean or stoichiometric premixed combustion. The expression given by Eq. (3) does not consider the mixture inhomogeneity within the flame, especially for the cases with variable diffusivities, and depends on species mass fraction in the unburnt gas which is not a constant value in the stratified flames [4]. By contrast, Eq. (4) does not need the species mass fraction values in the unburnt gas and can be applied as long as the reaction rate of progress variable and unburnt gas density values are provided. Hence, Eq. (3) is extended in our analysis to solve these issues as the consumption speed of a species α is defined by integrating the reaction rate $\dot{\omega}_\alpha$ in the flame normal direction, and unburnt density $\rho(\phi)_P^u$ and the mass fractions in the burnt and unburnt mixtures $Y_\alpha(\phi)_P$ are obtained from a corresponding (precalculated) homogeneous mixture flame calculation as:

$$S_{c,\alpha} = \int_{-\infty}^{+\infty} \frac{-\dot{\omega}_\alpha}{\rho(\phi)_P^u \cdot [Y_\alpha(\phi)_P^u - Y_\alpha(\phi)_P^b]} dx \tag{5}$$

Previous studies [8] used the definition given by Eq. (3), whereas the rewritten form of it in Eq. (4) becomes consistent with the extended consumption speed expression in Eq. (5). This extended formulation enables us to include an unambiguous definition of the species mass fraction in the burnt mixture, especially important for fuel-rich stratified flames. The simulations in this work employ the the extended definition of consumption speed of Eq. (5).

Our analysis also considers two flame thicknesses based on the gradients of the temperature ($\delta_{l,T}$) and of the progress variable ($\delta_{l,C}$):

$$\delta_{l,T} = \frac{T(\phi)_P^b - T(\phi)_P^u}{|\nabla T|_{max}}, \qquad \delta_{l,C} = \frac{1}{|\nabla C|_{max}} \tag{6}$$

The effects of stratification on the reaction-diffusion balance and local flame propagation can be analysed using the density-weighted displacement speed S_d^* [8] for the systems with Fickian diffusion:

$$S_d^* = \underbrace{\frac{\nabla \cdot (\rho D_C \nabla C)}{\beta}}_{T_1} + \underbrace{\frac{\dot{\omega}_C}{\beta}}_{T_2} + \underbrace{\frac{2\zeta^{-1}\rho D_C \nabla C \cdot \nabla \zeta}{\beta}}_{T_3} \tag{7}$$

The components T_1 and T_2 represent diffusion and reaction rate contributions, respectively, and T_3 represents the cross-dissipation component that accounts for the flux of mixture fraction normal to the flame. Interested readers are directed to Bray et al. [22] for the origin of the term T_3. The diffusivity of the progress variable and the density-weighted reaction progress variable magnitude are given as D_C and $\beta = \rho(\phi)_P^u |\nabla C|$, respectively. The diffusivity and the reaction rate of the species, which is used to define the progress variable, are used for the evaluation of D_C and $\dot{\omega}_C$, respectively. The density-weighted displacement speed is equal to the laminar burning velocity for unstretched premixed flames in one-dimension.

The cross-dissipation component T_3 in Eq. (7) needs to be corrected for the simulations with variable diffusivity assumption

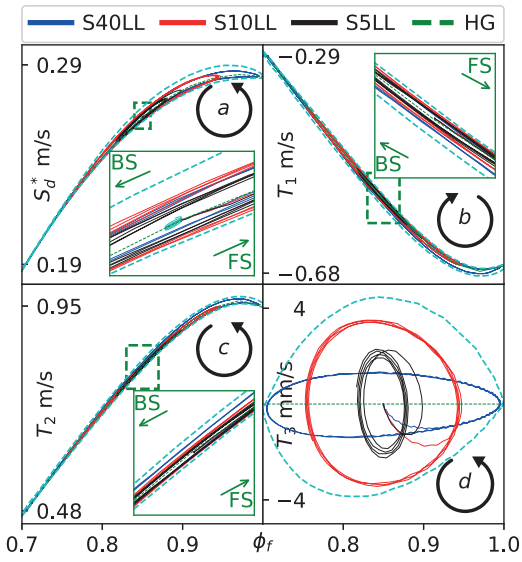

Fig. 2. Density-weighted displacement speed S_d^* (a) and its components T_{1-3} (b)–(d) over ϕ_f for equal diffusivities for $C = 0.8$ iso-line. Corresponding computations for homogeneous mixture are denoted as HG. Cyan lines denote the linearly stratified cases for comparison. (For interpretation of the references to color in this figure legend, the reader is referred to the web version of this article.)

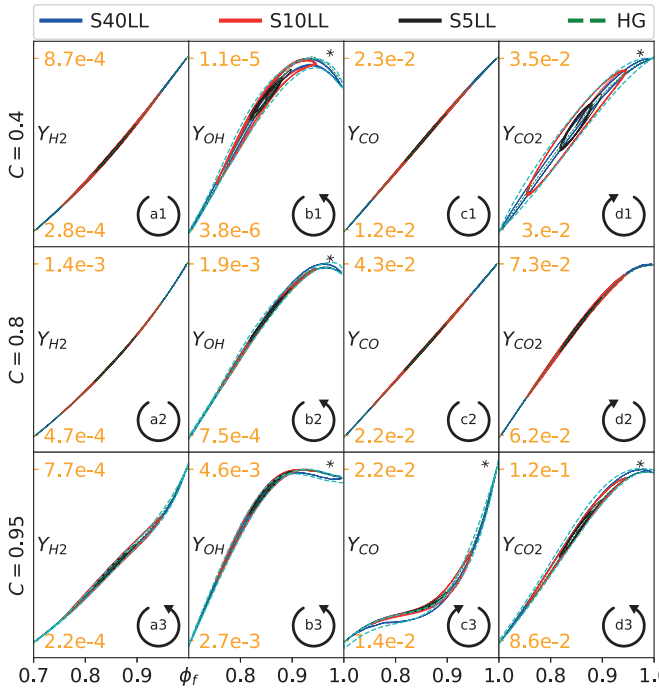

Fig. 3. Species mass fractions over ϕ_f for three zones with equal diffusivities. Corresponding computations for homogeneous mixture are denoted as HG. Cyan lines denote the linearly stratified cases for comparison. The star symbol marks significant results. (For interpretation of the references to color in this figure legend, the reader is referred to the web version of this article.)

since the equivalence ratio computed from the elemental mixture fraction is not uniform in the reaction zone of the flame (Fig. A.12) as previously reported by Bray et al. [22]. The correction of the cross-dissipation component T_3 requires precomputation of this term by elemental mixture fraction from a homogeneous mixture solution with a variable diffusivity assumption. The expression of S_d^* for the variable diffusivity assumption is:

$$S_d^* = \frac{\nabla \cdot (\rho D_C \nabla C)}{\beta} + \frac{\dot{\omega}_C}{\beta} + \frac{2\rho D_C \nabla C}{\beta}\left[\frac{\nabla \zeta}{\zeta} - \frac{\nabla \zeta(\phi)_P}{\zeta(\phi)_P}\right] \tag{8}$$

The mixture fraction and its gradient from the homogeneous mixture solution are denoted as $\zeta(\phi)$ and $\nabla\zeta(\phi)$, respectively. These two quantities, $\zeta(\phi)$ and $\nabla\zeta(\phi)$, use the elemental mass fraction definition (Appendix A) applied to the equivalent homogeneous mixture computation. This correction of cross-dissipation component T_3 in Eq. (8) can only be applied if the flame propagates in equivalence ratio gradient direction.

4. Stratified flame dynamics using equal diffusivities

The density-weighted displacement speed S_d^* and its components T_{1-3} defined in Eq. (7) are presented in Fig. 2: due to the stratification, these quantities are no longer unique function of equivalence ratio: they 'orbit' around the homogeneous mixture solutions, indicating a hysteresis. The area within the orbit or the deviation from the homogeneous mixture flame depends on the wavelength and amplitude of the stratification. The direction of the orbit (circular arrow in each figure) indicates the sign of the phase shift: a quantity ψ (e.g. S_d^* in Fig. 2(a)) lagging behind the equivalence ratio signal ϕ will show a counterclockwise orbit, unless the quantity ψ is computed from gradients (e.g. T_1 of S_d^* in Fig. 2(b)), which will experience the opposite effect.

All the components of S_d^* (i.e. T_1, T_2 and T_3) exhibit hysteresis, but orbit in different directions, and as a result, partially compensate each other. The high heat release behind the BS flame makes the reaction rate component orbit in a counter-clockwise direction, whereas, the diffusion component orbits in the opposite direction due to the steeper diffusive flux-gradient of the thinned flame. The flame burning towards the negative equivalence ratio gradient in BS mode causes the cross-dissipation component T_3 to orbit in counter-clockwise direction. Since this term is the first-order derivative of the equivalence ratio, the orbit shows an almost circular pattern.

The response of all of the components of S_d^* to the sinusoidal oscillations are similar to the ones in a linear mixture wave (cyan lines in Fig. 2). Similarly, the sinusoidal cases in FS mode show resemblance to the LFS case.The Term T_3 for the linear cases (LBS and LFS) do exhibit more or less circular T_3 distribution over the equivalence ratio space due to the linear variation of the mixture fraction gradient.

All of the analysed quantities, except the cross-dissipation component, show stronger hysteresis close to the stoichiometric mixture due to the higher heat release of the richer mixture that can support the flame more than the leaner mixtures with lower heat release. This explains the strong hysteresis towards the richer mixtures, but not at the locations where the equivalence ratio gradient attains its maximum magnitude.

The mass fractions of H_2, OH, CO and CO_2 are shown for the preheat, inner reaction and burnout zones in Fig. 3 for equal diffusivities. The responses of the composition oscillations to the sinusoidal cases resemble greatly to the linear ones, especially during the FS mode. The directions of the orbits seem to interchange between species and the flame zones. Hydrogen H_2 concentrations only exhibit hysteresis in the burnout zone. The preheat zone shows hysteresis mainly in terms of OH and CO_2 concentrations. The species concentrations in the inner reaction zone are almost hysteresis-free.

The concentration variations in the preheat zone are only limited for some of the species such as OH and CO_2, whereas most of the variations happen in the burnout zone. This should not be confused with the strength of the hysteresis since the species that are under a considerable phase shift in the preheat zone have a very low local concentration. However, for the species such as H_2 and CO that have locally similar concentrations both in preheat and

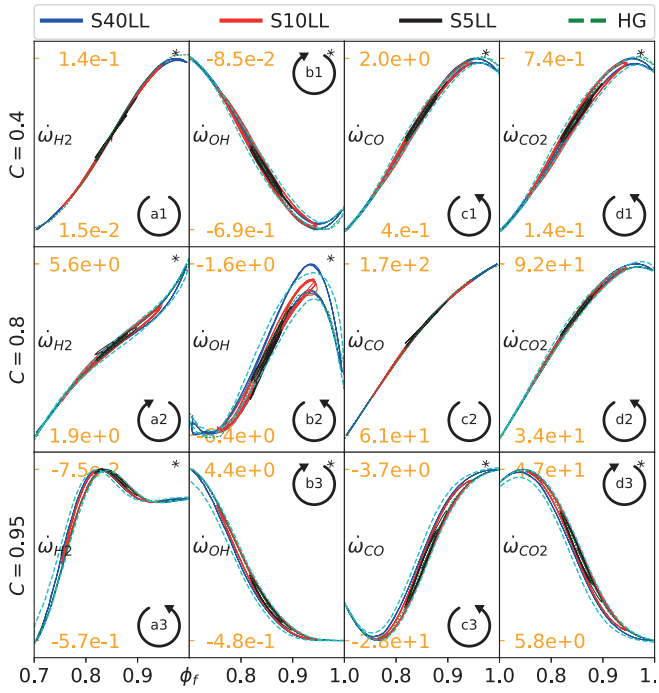

Fig. 4. Species reaction rates over ϕ_f for three zones with equal diffusivities. Corresponding computations for homogeneous mixture are denoted as HG. Cyan lines denote the linearly stratified cases for comparison. The star symbol marks significant results. (For interpretation of the references to color in this figure legend, the reader is referred to the web version of this article.)

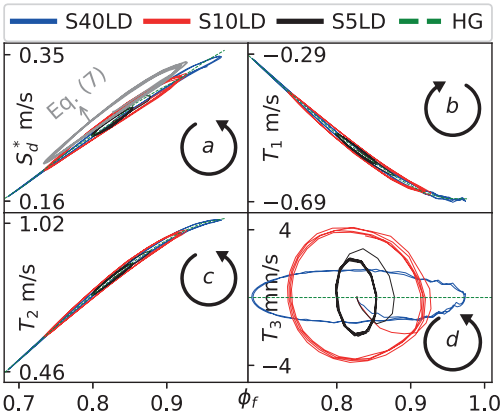

Fig. 5. Density-weighted displacement speed S_d^* (a) and its components T_{1-3} (b)–(d) over ϕ_f for variable diffusivities for $C = 0.8$ iso-line. The density-weighted displacement speed from Eq. (7) for S10LD is illustrated by the grey line for reference. Corresponding computations for homogeneous mixture are denoted as HG. (For interpretation of the references to color in this figure legend, the reader is referred to the web version of this article.)

burnout zones, the hysteresis effects are only visible in towards the burnout zone. The hysteresis effects for some species in the preheat zone have been similarly present in the cases with strain rate fluctuations [4], thus exhibiting similarities to the present case without strain.

The reaction rates of the aforementioned species are shown in Fig. 4. Hydrogen H_2 and the hydroxyl radical OH exhibit a strong hysteresis in both the preheat and inner reaction zones and some hysteresis in the burnout zone. The H_2 and OH species in the inner reaction zone seem to be the most affected species due to equivalence ratio stratification. The reaction rates of CO and CO_2 exhibit a minor hysteresis in the inner reaction zone. The burnout zone, however, exhibits a hysteresis for all of the reaction rates. The species mass fractions and the reaction rates show the largest hysteresis around $\phi = 0.9$.

In the inner reaction zone, it seems that the sinusoidal reaction rate profiles are constrained from the upper and lower limits of the equivalence ratio, thus, the reaction rates of the sinusoidal case, e.g. OH, deviate from the so-called limits of linear cases towards the mean equivalence ratio $\overline{\phi}$. This observation can partially be seen in the burnout zone.

During the BS mode, the excessive heat and products behind the flame support the reaction zone, leading to flame thinning. The thermal diffusion towards the interior of the flame creates additional highly reactive species such as O, H and OH. The increased local heat release and addition of the reactive species augment the consumption rate of reactants (mostly O_2). Hence, the formation of products in the preheat and inner reaction zones are enhanced (orbit in a counter-clockwise direction). However, the quickly depleted reactants limit the formation of the products in the burnout zone (shift of orbit to clockwise direction). The changes in the preheat zone also affect the ignition-related species (CH_2O and HO_2), as illustrated in Fig. S3 of the supplementary material.

5. Stratified flame dynamics using mixture-average diffusivities

The effects of the variable diffusivity assumption on stratified flames have been investigated for turbulent flames by DNS in two [23] and three-dimensions [24] and by experiments [25]. A detailed study of the effect of variable diffusivity on flame chemistry has been performed by Hilbert et al. [26]. These analyses suggest that it is worthwhile to investigate the cases investigated here again for variable diffusivities to examine their influences on the results. The local mixture fraction now exhibits slight deviations within the flame due to the faster transport of light species (as in Fig. A.12). This yields slightly lower equivalence ratios in the inner reaction zone than in the preheat zone. Therefore, the equivalence ratio of the flame ϕ_f is recomputed on the investigated progress variable iso-line.

The density-weighted displacement speed S_d^* for $C = 0.8$ is presented in Fig. 5 for variable diffusivities. The density-weighted displacement speed S_d^* in Fig. 5(a) is always higher than the equivalent homogeneous mixture value due to the uncorrected positive cross-dissipation component T_3 from Eq. (7). This issue is avoided by the proposed density-weighted displacement speed S_d^* according to Eq. (8). Neglecting this correction yields 4.4% overestimated density-weighted displacement speed.

The hysteresis of these three terms has similar strengths and their orbit directions remain unchanged, however, the hystereses are now clearly more prominent. The phase shift of Term T_3 using variable diffusivities is a factor of four less than the shift when using equal diffusivities. However, the stronger hysteresis in diffusion and reaction rate components using variable diffusivities compensates this loss from Term T_3.

The mass fractions of H_2, OH, CO and CO_2 are presented in Fig. 6 for the preheat, inner reaction and burnout zones. In the preheat zone, the inclusion of variable diffusivities yields a hysteresis for the species that have not exhibited hysteresis with equal diffusivities. The H_2 and OH species are explicitly analysed for the preferential diffusion effects in stratified flames. In the preheat zone, the CO_2 concentration of the strongly stratified cases (S5LD and S10LD) follows a different path than for the weakly stratified S40LD case. The hysteresis of the diffusive fluxes of CO_2 is probably responsible for this behaviour. The light species H_2 (and H) also show a prominent increase of the hysteresis due to the preferential diffusion, but only towards the preheat and inner reaction zones. The concentration of the species H_2, OH, CO are slightly higher in

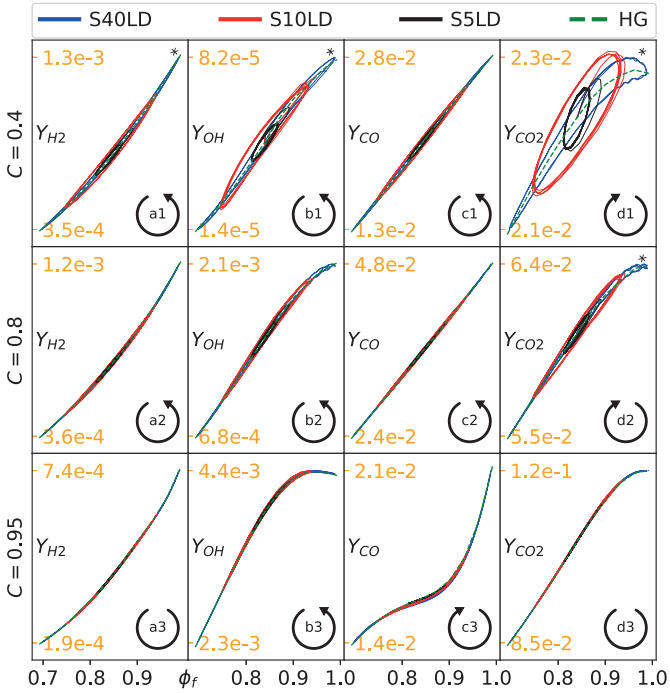

Fig. 6. Species mass fractions over ϕ_f for three zones with variable diffusivities. Corresponding computations for homogeneous mixture are denoted as HG. The star symbol marks significant results. (For interpretation of the references to color in this figure legend, the reader is referred to the web version of this article.)

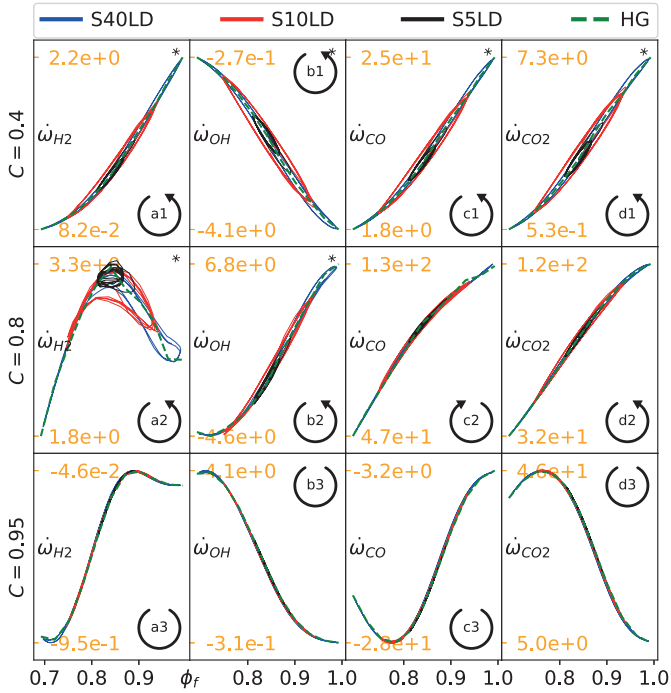

Fig. 7. Species reaction rates over ϕ_f for three zones with variable diffusivities. Corresponding computations for homogeneous mixture are denoted as HG. The star symbol marks significant results. (For interpretation of the references to color in this figure legend, the reader is referred to the web version of this article.)

these zones compared to the cases with equal diffusivities, which leads to strengthening of the observed hysteresis.

Strong hysteresis of the species reaction rates in the preheat zone using variable diffusivities follows the trend observed in the species concentrations. During the BS mode, the consideration of the variable diffusivities greatly enhances the production rates of highly reactive species O, H, H_2 and OH. This high reaction rates in the preheat zones using variable diffusivity assumption are expected, but, this is now combined with stronger hysteresis as well. This enhanced production of reactive species leads to a significant increase in the consumption rate of the fuel and air, giving rise to eventual flame thinning. The enhanced diffusive fluxes of the thinned flame are likely to be responsible for suppressing the hysteresis in the burnout zone. It should be noted that the major product species H_2O follows a similar trend as CO and CO_2, and was omitted for brevity.

The response of the unstrained stratified flames to the low-frequency mixture oscillations exhibits quasi-steady behaviour for the cases with equal diffusivities, as similar to the strained stratified flames [6]. Considering variable diffusivities reveals that the light species, e.g. H_2, in the inner reaction zone exhibits an unsteady behaviour, which implies that some statistical variations in the orbits during the wave-cycles are likely to be evident (Fig. 7(a2)). Only the light species H and H_2 for cases with slightly higher oscillation-frequency show this trend. This sole observation could not have been made for the flames under compressible strain, which suppresses the thermal activity of the light species due to enhanced diffusion caused by strain. However, this observation might not play a significant role in turbulent stratified flame modelling, as most of the features of a stratified flame that burns towards the mixture gradient direction, can be well-captured with a reduced chemical mechanism and equal diffusivity assumption.

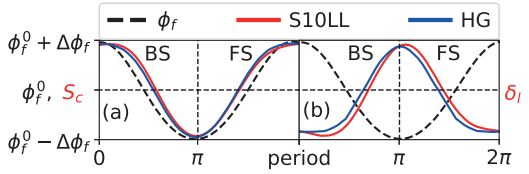

Fig. 8. Consumption speed (a) and flame thickness (b) response to the sinusoidal equivalence ratio wave for equal diffusivity. The amplitudes are qualitative. Period is discretized into BS and FS modes. Corresponding computations for homogeneous mixture are denoted as HG. (For interpretation of the references to color in this figure legend, the reader is referred to the web version of this article.)

6. Implications for consumption speed and flame thickness

Simulations of combustion often require dimension reduction techniques, e.g. [20]. For example, the popular reduction method tabulation techniques relies on an accurate description of flame propagation speed and thermal flame thickness. In this section, the popular methods to compute the flame speed and thickness and the consequences of neglecting stratification effects on the results will be discussed. Once again, we stress that this analysis is only carried out for flames propagating towards the equivalence ratio gradient.

The responses of the consumption speed S_c (based on oxidiser mass fraction) and flame thickness δ_l (based on temperature gradient) to the sinusoidal oscillations of equivalence ratio are illustrated in Fig. 8. The time series of these scalars are compared to the values that would result from the equivalent homogeneous mixture computations. Both the consumption speed and the flame thickness are shifted to the right, meaning that their responses are delayed. The estimated phase shifts of S_c and $\delta_{l,T}$ are 5^o and 9^o, respectively.

The sinusoidal equivalence ratio and its responses (consumption speed, flame thickness) intersect in every maximum and minimum of ϕ (where the local stratification is zero), which is only possible

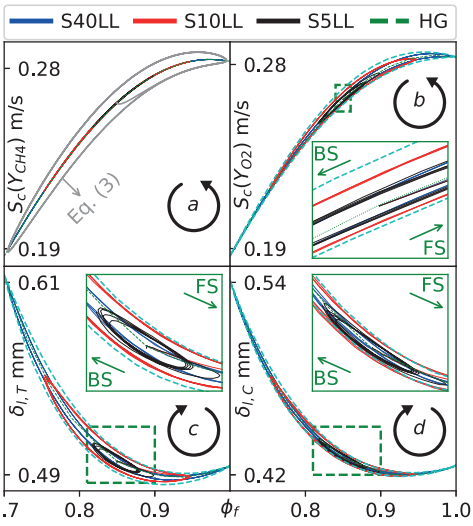

Fig. 9. Consumption speed based on fuel (a) and oxidiser (b) and flame thickness based on the gradients of T (c) and C (d) over ϕ_f for equal diffusivities. Corresponding computations for homogeneous mixture are denoted as HG. Consumption speed based on fuel computed with Eq. (3) for S40LL is illustrated with grey line as an example. Cyan lines denote the linearly stratified cases for comparison. BS and FS modes are shown. The circular arrows indicate the direction of the orbit. (For interpretation of the references to color in this figure legend, the reader is referred to the web version of this article.)

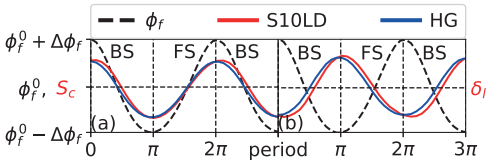

Fig. 10. Consumption speed (a) and flame thickness (b) response to the sinusoidal equivalence ratio wave for variable diffusivity. The amplitudes are qualitative. Period is discretized into BS and FS modes. Corresponding computations for homogeneous mixture are denoted as HG. (For interpretation of the references to color in this figure legend, the reader is referred to the web version of this article.)

if the responses have a higher amplitude. These are actually deformed waves, with distinct phase shifts. This deformation alters the mass and energy balance of the system, hence, some quantities respond quicker to the equivalence ratio signal ϕ (e.g. CO_2 in Figs. 3 or 6). The mean direction of the shift has been reported wherever necessary. Since the cases presented in this work use a constant wave-velocity, the time for the fuel to travel through the flame decreases with increasing λ. However, the phase shift for the cases with different oscillation frequencies is of the same magnitude. This is contrary to the previous findings for strained flames, where the phase shift is amplified with decreasing residence time of the fuel in the flame [6]. The diffusion could attenuate the phase shift under high frequencies [6], but not for the present cases with considerably low frequencies. Oscillation frequency dependency on the stratification effects are discussed in Appendix C.

Figure 9 (a) shows that the consumption speed based on fuel reaction rate does not exhibit any hysteresis, whereas the consumption speed based on oxidiser reaction rate (Fig. 9(b)) is clearly influenced by the stratification: it deviates approximately 1% from the homogeneous mixture case. The absence of the hysteresis in the consumption speed can be attributed to the employed modified definition of the consumption speed in Eq. (5), where a conventional consumption speed formulation given in Eq. (3) does exhibit a hysteresis (i.e. grey line in Fig. 9(a)). When assuming equal diffusivities, the phase of the flame response to the oscillations synchronises almost perfectly to the locally integrated fuel reaction rate and the unburnt mass fraction. The integrated unburnt density does not influence the hysteresis since its local variations are negligible. If the mass flow-rate of the oxidiser were varied to generate the equivalence ratio stratification instead of the mass flow-rate of the fuel, then Eq. (5) with the oxidiser properties would yield a hysteresis-free behaviour, but, only when using equal diffusivities for species. Furthermore, the BS mode appears to cause a larger deviation from the homogeneous mixture case than the FS mode.

Figure 9 (c) and (d) shows the large hysteresis in the flame thickness, with deviations of up to 3% from the homogeneous mixture case. The thickness based on temperature gradient exhibits a stronger hysteresis than the one based on the progress variable gradient. This is associated to the thickness of the temperature and the progress variable layers, where the consumption speed layer of the oxidiser is slightly narrower than the thermal zone, which is previously discussed for strained flames [6].

The sinusoidal cases are compared against the cases with linear mixture stratification LBS and LFS for equal diffusivities. The cyan lines in Fig. 9 indicates that the response of the flame to a linear stratification layer is very similar to a sinusoidal one. Since the stratification thicknesses δ_S of the linear cases are considerably lower than the sinusoidal ones (a factor of four smaller), the phase shift for linear cases is expected to be much stronger than the sinusoidal ones, as observed for hydrogen flames [9]. The LBS case with BS properties exhibits only slightly stronger hysteresis than the sinusoidal one, whereas the hysteresis strength of the LFS and sinusoidal wave during the FS mode are almost the same. The hysteresis strength depends on the deviation of the stratified mixture results from the equivalence homogeneous mixture results, and is not correlated to the stratification strength. This supports the previous findings for the strong correlation between the stratification effects and the heat release [8]. However, we do not observe a strong correlation between the stratification thickness δ_S and the hysteresis strength in these unstrained cases. Due to the higher propagation speeds and thinner reaction zones, more efficient combustion is expected for the stratified flames that burn in a wider equivalence ratio space close to the stoichiometry, stressing that this observation is made for unstrained one-dimensional configurations.

The responses of the consumption speed (based on oxidiser mass fraction) and flame thickness (based on temperature gradient) to the sinusoidal oscillations are illustrated in Fig. 10, but this time for variable diffusivities. The time series of these scalars are compared to the values that would result from the equivalent homogeneous mixture computations. The direction of the shift is the same as in the equal diffusivity case (Fig. 8), however, the magnitude of the shifts are now more apparent: the estimated phase angles of S_c and δ_l between these waves are 7^o and 16^o, respectively.

Figure 11 shows the consumption speed S_c and the flame thickness δ_l resulting from the sinusoidal equivalence ratio variation. A hysteresis is now apparent for the consumption speed based on fuel reaction rate, which can deviate up to 4% from the equivalent homogeneous mixture case. The phase shift of the consumption speed is clearly reduced by employing the modified definition of the consumption speed in Eq. (5) (conventional definition is the grey line in Fig. 9(a)). The hysteresis of the consumption speed based on oxidiser reaction rate is again larger than the fuel-based one. Similar to the equal diffusivity cases, the hysteresis is more prominent for the S10LD case than in the S5LD and S40LD cases. The flames for the variable diffusivity calculations thicken more compared to their equal diffusivity counterparts, and deviations can be as high as 7%. These hystereses are enhanced by a factor of two compared to the equal diffusivity cases, while, the directions of the orbits remain the same. However, the response

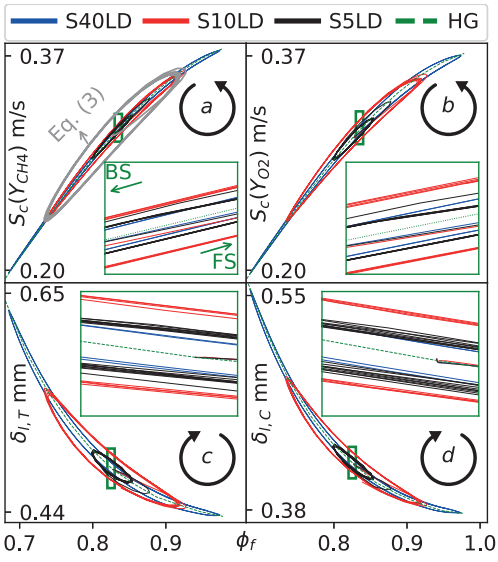

Fig. 11. Consumption speed based on fuel (a) and oxidiser (b) and flame thickness based on T (c) and C (d) over ϕ_f for variable diffusivities. Corresponding computations for homogeneous mixture are denoted as HG. Consumption speed based on fuel computed with Eq. (3) for S10LD is illustrated with grey line as an example. (For interpretation of the references to color in this figure legend, the reader is referred to the web version of this article.)

of the flame to different stratification thicknesses δ_S when using equal or variable diffusivities are quite similar, only amplified in strength, contrary to the stratified hydrogen flames [9].

Using the conventional definition of the consumption speed (i.e. Eq. (3)) exhibits large departure from the laminar flame speed of the equivalent homogeneous mixture by a large margin, which can be avoided by the extended consumption speed definition (Eq. (5)). For the laminar flame thickness, the choice of the species is of great importance for the stratified flames since the thickness of the progress variable layer and the strength of the hysteresis are correlated. One might argue, however, that the flame thickness computed with the gradient of the temperature is perhaps not appropriate for stratified flames due to the non-unique definition of the adiabatic flame temperature.

7. Conclusions

Detailed one-dimensional simulations of unsteady unstrained laminar flames subjected to both linear and sinusoidal equivalence ratio perturbations have been conducted. Greater amplitudes and shorter wavelengths of sinusoidal equivalence ratio variations led to stronger stratification effects and subsequently gave rise to greater phase shifts between the equivalence ratio oscillations and the responses of species concentrations and flame properties. However, in the absence of compressible strain, the stratification effects in high frequencies were limited to the diffusive fluxes.

When shown in equivalence ratio space, the phase shift caused a hysteresis or an orbit. The consumption speed, flame thickness and density-weighted displacement speed showed strong hysteresis in the equivalence ratio space. The trajectories of the leading order components of the density-weighted displacement speed were in opposite directions in the equivalence ratio space, partially compensating the hysteresis effect for the net density-weighted displacement speed.

The presented results demonstrated that the unstrained flames propagating into stratified mixtures exhibit a significant amount of unsteady response, even for relatively low frequencies. The phase response caused by the stratification oscillations is reflected in deformed waves as the system tried to balance itself. As a result, the major species mass fractions in the preheat zone showed quicker responses than the equivalence ratio signal.

The stratification effects were significantly enhanced in strength when the equal diffusivity assumption was replaced by more realistic (mixture-average) diffusivity assumption. However, the qualitative nature of the results does not change significantly as a result of the changes in species diffusivity treatment and thus it can be expected that these effects will not play a significant role in the simulation of turbulent stratified flames. However quantitatively, the preferential diffusion enhances the stratification effects by a factor of two, especially important for the accurate predictions of flame propagation.

It was demonstrated here that eliminating ambiguous quantities are advantageous for the analysis of unsteady responses of the consumption speed and flame thickness. The progress variable choice had a substantial impact on the strength of the hysteresis, which depended on the thickness of the progress variable layer. A correction to the displacement speed was suggested and it has been demonstrated to remove the dependency between the displacement speed and the definition of the equivalence ratio in the flame. This correction could be particularly useful for the modelling of the stratified flames under the assumption of variable diffusivities.

The evaluation of the detailed and the reduced mechanism for the unsteady responses led to stratification effects of the same strength, hence, numerical simulations of the stratification effects can be conducted using reduced chemical mechanisms without sacrificing the accuracy.

Acknowledgments

The authors gratefully acknowledge the financial support by DFG (Proj. No.: 393710272, KE 1751/13-1) and EPSRC (EP/R029369/1) and the compute time on magnitUDE, Duisburg (DFG INST 20876/209-1 FUGG) and on ARCHER, Edinburgh (e305 – UKCTRF).

Appendix A. Mixture fraction

The mixture fraction ζ based on elemental mass fraction definition proposed by Bilger [21] and applied to stratified flames by Cruz et al. [5] is given as:

$$\zeta = \frac{\frac{\zeta_C}{\nu_C W_C} + \frac{\zeta_H}{\nu_H W_H} + 2\frac{\zeta_{O,2-Z_O}}{\nu_O W_O}}{\frac{\zeta_{C,1}}{\nu_C W_C} + \frac{\zeta_{H,1}}{\nu_H W_H} + 2\frac{\zeta_{O,2}}{\nu_O W_O}} \tag{A.1}$$

This formulation is valid for a general hydrocarbon combustion with nitrogen content used as a diluent. In Eq. (A.1), ν_i is the stoichiometric coefficient, W_i is the molecular weight, ζ_i is the mass fraction of element i inside an imaginary stream j, where fuel and oxidiser streams are denoted with subscript 1 and 2, respectively. Methane as the hydrocarbon has these values $\nu_C = 1$, $\nu_H = 4$ and $\nu_O = 4$. Elemental mass fractions ζ_i are computed by adding the contributions of all species that contain the element i, as $\zeta_i = (W_i/\rho)\sum_{k=1}^{N_{species}} n_{i,k}C_k$, where $n_{i,k}$ is the number of atoms and C_k is the molar concentration of species k. The fuel and air stream of elemental mass fractions are then $Z_{C,1} = W_C/(W_C + 4W_H)$, $Z_{H,1} = 4W_H/(W_C + 4W_H)$ and $Z_{O,2} = W_O/(W_O + 0.79/0.21W_N)$. The equivalence ratio ϕ can be defined using a stoichiometric mixture fraction of $\zeta_{ST} = 0.055$ for methane-air combustion as:

$$\phi = \frac{\zeta}{1-\zeta}\frac{1-\zeta_{ST}}{\zeta_{ST}} \tag{A.2}$$

The equivalence ratio ϕ defined by Eq. (A.2) has a constant value in the reaction zone for simulations using equal diffusivity

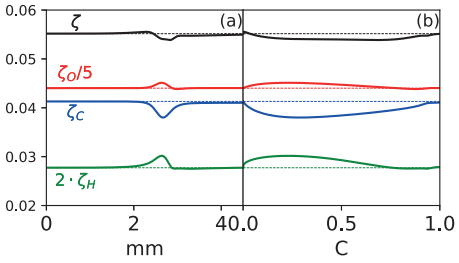

Fig. A.12. Bilger's elemental mixture fraction ζ [21] with elemental mass fractions Z_i over the physical space (a) and the progress variable C (b) for a stoichiometric methane-air premixed mixture flame. Straight and dashed lines represent the cases with mixture-averaged and equal diffusivity assumptions, respectively. (For interpretation of the references to color in this figure legend, the reader is referred to the web version of this article.)

assumption. However, the elemental mass fractions show variations when using mixture-averaged diffusivity assumption, as presented for stoichiometric methane-air flame in Fig. A.12. Thus, the simulations that apply variable diffusivities must account for the non-uniformity of ϕ over the reaction zone, as discussed in this work.

Appendix B. Mechanism comparison

Figure B.13 presents the comparisons between the mechanisms developed by Lu and Law [18] (LL19) and GRI3.0 [19] for equal diffusivity assumption. By using a reduced mechanism, a speed-up of a factor of four is achieved compared to GRI3.0. As can be seen in Fig. B.13, both mechanisms are in very good agreement in terms of hysteresis strength.

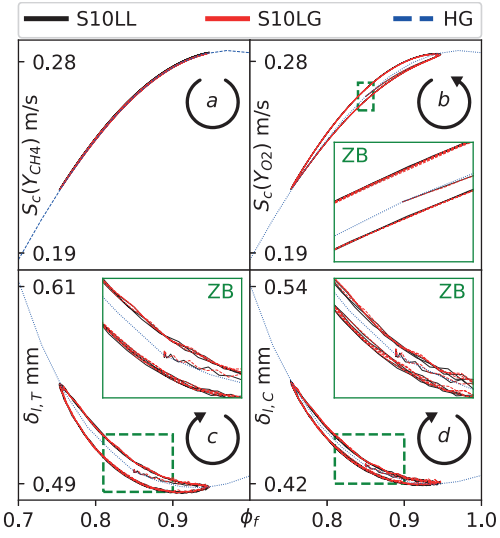

Fig. B.13. Consumption speeds based on fuel (a) and oxidiser (b) and flame thicknesses based on temperature (c) and progress variable (d) with ϕ_f using equal diffusivities with different reaction mechanisms. The corresponding homogeneous mixture computations for the same flame equivalence ratio ϕ_f are denoted as HG. (For interpretation of the references to color in this figure legend, the reader is referred to the web version of this article.)

Appendix C. Cut-off frequencies

Non-dimensional stratification thickness δ_S/δ_l and maximum attenuation of the density-weighted displacement speed $A(S_d^*)$ over the tested frequencies are demonstrated in Fig. C.14. The maximum attenuation is given in percentage difference of a scalar in a stratified mixture flame to the corresponding homogeneous mixture

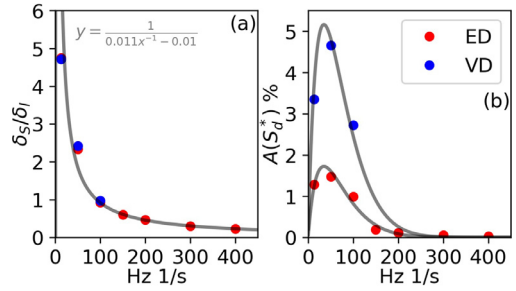

Fig. C.14. Non-dimensional stratification thickness (a) and maximum attenuation of the density-weighted displacement speed S_d^* (b) over the tested frequencies. Black and red dots represent the cases using equal and variable diffusivities, respectively. (For interpretation of the references to color in this figure legend, the reader is referred to the web version of this article.)

flame calculation. The frequency-domain in Fig. C.14 is constructed using seven and three samples from equal and variable diffusivity cases, respectively.

Figure C.14 (a) shows that the non-dimensional stratification thickness δ_S/δ_l rapidly reduces up to 200 Hz. For frequencies higher than 200 Hz, the diffusion attenuation limits the equivalence ratio gradients. Hence, the stratification thickness can assume small values as the diffusion limit in the absence of compressible strain. It is also evident that the stratification thickness δ_S for both equal and variable diffusivities follow the same trend.

Two cut-off frequencies can be identified from Fig. C.14(b). The frequency when the $A(S_d^*)$ becomes maximum is the lower cut-off frequency, and the upper cut-off frequency is when $A(S_d^*)$ is as low as 0.1%. The lower cut-off limit is projected as 35 Hz for both equal and variable diffusivity assumptions. It is estimated that the variable diffusivity cases have a factor of two larger maximum attenuation than the equal diffusivity ones, as a result, the upper cut-off frequencies using variable diffusivities is estimated 25 Hz more than the upper cut-off limit using equal diffusivities. Compared to the theoretical upper cut-off limit f^u of 5000 Hz estimated for the strained methane-air mixture flames at $\tilde{\phi}$ as $f^u = \ln(0.1)^2 S_L^2/\pi/D$ [6], the upper cut-off frequency for unstrained flames is as low as 250 Hz due to the action of the diffusive fluxes.

Supplementary material

Supplementary material associated with this article can be found, in the online version, at doi:10.1016/j.combustflame.2020.06.009.

References

[1] A.N. Lipatnikov, Stratified turbulent flames: recent advances in understanding the influence of mixture inhomogeneities on premixed combustion and modeling challenges, Progr. Energy Combust. Sci. 62 (2017) 87–132.
[2] F. Seffrin, F. Fuest, D. Geyer, A. Dreizler, Flow field studies of a new series of turbulent premixed stratified flames, Combust. Flame 157 (2) (2010) 384–396.
[3] M.S. Sweeney, S. Hochgreb, M.J. Dunn, R.S. Barlow, The structure of turbulent stratified and premixed methane/air flames i: non-swirling flows, Combust. Flame 159 (9) (2012) 2896–2911.
[4] F.N. Egolfopoulos, C.S. Campbell, Unsteady counterflowing strained diffusion flames: diffusion-limited frequency response, J. Fluid Mech. 318 (1996) 1–29.
[5] A.P. Da Cruz, A. Dean, J. Grenda, A numerical study of the laminar flame speed of stratified methane/air flames, Proc. Combust. Inst. 28 (2) (2000) 1925–1932.
[6] R. Lauvergne, F.N. Egolfopoulos, Unsteady response of C3H3/Air laminar premixed flames submitted to mixture composition oscillations, Proc. Combust. Inst. 28 (2) (2000) 1841–1850.
[7] T. Kang, D.C. Kyritsis, Departure from quasi-homogeneity during laminar flame propagation in lean, compositionally stratified methane–air mixtures, Proc. Combust. Inst. 31 (1) (2007) 1075–1083.
[8] E.S. Richardson, V. Granet, A. Eyssartier, J. Chen, Effects of equivalence ratio variation on lean, stratified methane–air laminar counterflow flames, Combust. Theor. Model. 14 (6) (2010) 775–792.
[9] X. Shi, J.-Y. Chen, Z. Chen, Numerical study of laminar flame speed of fuel-stratified hydrogen/air flames, Combust. Flame 163 (2016) 394–405.

[10] C. Galizzi, D. Escudié, Experimental analysis of an oblique laminar flame front propagating in a stratified flow, Combust. Flame 145 (3) (2006) 621–634.
[11] R. Sankaran, H.G. Im, Dynamic flammability limits of methane/air premixed flames with mixture composition fluctuations, Proc. Combust. Inst. 29 (1) (2002) 77–84.
[12] O. Badr, G. Karim, Flame propagation in stratified methane-air mixtures, J. Fire Sci. 2 (6) (1984) 415–426.
[13] P. Vena, B. Deschamps, G. Smallwood, M. Johnson, Equivalence ratio gradient effects on flame front topology in a stratified iso-octane/air turbulent v-flame, Proc. Combust. Inst. 33 (1) (2011) 1551–1558.
[14] A.M. Kempf, B.J. Geurts, J.C. Oefelein, Error analysis of large-eddy simulation of the turbulent non-premixed sydney bluff-body flame, Combust. Flame 158 (12) (2011) 2408–2419.
[15] E. Inanc, M.T. Nguyen, S. Kaiser, A.M. Kempf, High-resolution LES of a starting jet, Comput. Fluids 140 (2016) 435–449.
[16] E. Inanc, F. Proch, A. Kempf, Studying transient jet flames by high-resolution LES using premixed flamelet chemistry, DLESXI (2019) 237–243.
[17] E. Inanc, A.M. Kempf, Numerical study of a pulsed auto-igniting jet flame with detailed tabulated chemistry, Fuel 252 (2019) 408–416.
[18] T. Lu, C.K. Law, A criterion based on computational singular perturbation for the identification of quasi steady state species: a reduced mechanism for methane oxidation with no chemistry, Combust. Flame 154 (4) (2008) 761–774.
[19] G.P. Smith, et al. 2000, (combustion.berkeley.edu/gri-mech).
[20] F. Proch, P. Domingo, L. Vervisch, A.M. Kempf, Flame resolved simulation of a turbulent premixed bluff-body burner experiment. part i: analysis of the reaction zone dynamics with tabulated chemistry, Combust. Flame 180 (2017) 321–339.
[21] R.W. Bilger, The structure of diffusion flames, Combust. Sci. Technol. 13 (1976) 155–170.
[22] K. Bray, P. Domingo, L. Vervisch, Role of the progress variable in models for partially premixed turbulent combustion, Combust. Flame 141 (4) (2005) 431–437.
[23] H.N. Najm, O.M. Knio, P.H. Paul, Role of transport properties in the transient response of premixed methane/air flames, Proc. Combust. Inst. 29 (2) (2002) 1713–1720.
[24] C. Bruno, V. Sankaran, H. Kolla, J.H. Chen, Impact of multi-component diffusion in turbulent combustion using direct numerical simulations, Combust. Flame 162 (11) (2015) 4313–4330.
[25] R.S. Barlow, M.J. Dunn, M.S. Sweeney, S. Hochgreb, Effects of preferential transport in turbulent bluff-body-stabilized lean premixed ch4/air flames, Combust. Flame 159 (8) (2012) 2563–2575.
[26] R. Hilbert, F. Tap, H. El-Rabii, D. Thvenin, Impact of detailed chemistry and transport models on turbulent combustion simulations, Progr. Energy Combust. Sci. 30 (1) (2004) 61–117.